Characterization of clasts in the Glen Torridon region of Gale crater observed by the Mars Science Laboratory Curiosity Rover

Sabrina Khan (0000-0003-4212-4848)[1], Kathryn Stack (0000-0003-3444-6695)[2], and R. Aileen Yingst (0000-0002-0628-4265)[3] , Kristin Bergmann (0000-0002-6106-2059)[1]

[1]Massachusetts Institute of Technology, Department of Earth, Atmospheric, and Planetary Sciences, 77 Massachusetts Avenue, 54-918, Cambridge, MA 02139

[2]Jet Propulsion Laboratory, California Institute of Technology, 4800 Oak Grove Drive, Pasadena, CA 91109

[3]Planetary Science Institute, 1700 East Fort Lowell, Tucson, AZ

Corresponding Author:

Sabrina Khan

sabrinayasmeenkhan@gmail.com

Key Points:

- Clasts are abundant across the surface of Glen Torridon and support the presence of a distinct erosional regime in this area of Mount Sharp
- 8 distinct clast types are identified throughout the region with different types representing distinct stages along the erosional continuum
- Clasts are locally sourced and represent erosional and deflationary remnants of the Jura and Knockfarril Hill members

Abstract
Granule- to cobble- sized clasts in the Glen Torridon region of Gale crater on Mars were studied using data captured by NASA's Mars Science Laboratory Curiosity rover between sols 2302 and 2593. The morphology and composition of clasts have the potential to reveal the nature and extent of erosional processes acting in a region. In this study, measurements of shape, size, texture and element abundance of unconsolidated clasts within lower Glen Torridon were compiled. Eight primary clast types were identified, all of which are sedimentary and can be compositionally linked to local bedrock, suggesting relatively short transport distances. Several clast types exhibit signs of aeolian abrasion, such as facets, pits, flutes and grooves. These results indicate that clasts are primarily the product of bedrock degradation followed by extensive aeolian wear.

Plain Language Summary
Clasts are loose fragments produced by the breakdown of rock, which can be transported and reshaped by forces like water, wind and gravity. Clast shape, size and texture are useful indicators of the clast's origin and the forces that have transported and modified it over time. The Glen Torridon region of Gale crater, field site for NASA's Mars Science Laboratory Curiosity rover, is home to an abundance of granule- to cobble-sized clasts. Between martian days ('sols') 2300 and 2593, Curiosity captured images and compositional data of Glen Torridon clasts along the traverse. In this study, measurements of shape, size, texture and composition of Glen Torridon clasts were compiled for characterization, and to determine their origin and erosional history. Eight primary clast types were identified, all of which are sedimentary rock and are similar in composition to the local bedrock, suggesting most clasts were transported short distances. Glen Torridon clasts exhibited signs of wind-driven abrasion, such as facets, pits, flutes and grooves. These results indicate that clasts in Glen Torridon are primarily the product of bedrock fragmentation followed by extensive wind-abrasion.

Index Terms: Mars (6225), Erosion and weathering (5415), Surface materials and properties (5470)

Keywords: Clasts, Mars Science Laboratory, Gale crater, Glen Torridon, Aeolian Processes, Morphology

1 Introduction

In-place bedrock geology provides a reliable record of depositional and erosional history, but unconsolidated clasts can also be used to ascertain the dominant modes of modification and transport over local and regional scales. Clasts can log the nature, intensity, and evolution of erosional environments and transport processes they encounter from the time of their formation to the point of deposition within quantifiable parameters such as size, roundness, and shape. Compositional trends and lithological characteristics can be used as further evidence to tie a clast to its source region. In the case of robotic planetary exploration, clast characterization has the added benefit of aiding and informing rover safety evaluation, as clasts can pose hazards for traversibility. Clasts can also be used as a proxy for bedrock that would otherwise be inaccessible to a rover. Since landing, the Mars Science Laboratory Curiosity rover has been systematically acquiring images of clasts using the Mastcam and MARDI cameras in the nearfield around the rover at the completion of each of the rover's drives. Syntheses of these clast survey observations in Gale crater were performed at Bradbury Rise and along the traverse to Yellowknife Bay (Yingst et al., 2010, 2013, 2016) where unconsolidated clasts were abundant. Building on the work of

Yingst et al. (2013, 2016), this study focuses on the characterization of clasts in the Glen Torridon region of Gale crater, where the Curiosity rover encountered an unusually dense collection of granule- to cobble- sized clasts distributed across a region known for its clay-bearing spectral signatures from orbit (Fraeman et al., 2016; Milliken et al., 2010, 2014) and on the ground (Bristow et al., 2019), and the presence of decameter long-ridges interpreted as periodic bedrock ridges (PBRs) (Stack et al., 2019, this issue). The purpose of this study is to characterize the clasts in Glen Torridon in order to determine their origin and history, including the mechanisms of formation and modification, and to identify their relationship to the Glen Torridon PBRs.

1.1 Geologic Context

Gale crater is a 155 km diameter impact crater situated along the martian crustal dichotomy boundary, a topographic feature which bisects the heavily cratered southern highlands and the younger northern plains. The crater, which is thought to have formed 3.8-3.6 Ga (Deit et al., 2013; Thomson et al., 2011), contains within it a 5 km thick central mound of sedimentary rock known as Aeolis Mons (informally referred to as Mount Sharp). Gale's extensive record of sustained aqueous activity, particularly the transition from clay-bearing to sulfate-bearing strata observed within the lower reaches of Mount Sharp, motivated its selection as the landing site for the MSL mission (Grotzinger et al., 2014, 2015). Since landing on Bradbury Rise in August 2012, Curiosity has been exploring a thick sedimentary succession of fluvial, fluvial-deltaic, lacustrine and aeolian rocks. Beginning around martian day ("sol") 700, Curiosity traversed into the Murray formation, an interval of the Mount Sharp group comprised primarily of finely-laminated mudstones. Murray formation mudstones have been interpreted to be associated with deposition in a low-energy lacustrine environment that extends nearly continuously from the Pahrump Hills outcrop to this study's region of interest in Glen Torridon (Edgar et al., 2020; Fedo et al., 2017; Grotzinger et al., 2015; Rivera-Hernández et al., 2019; Stack, Grotzinger, et al., 2019). During this exploration of the Murray formation, the Curiosity rover has also encountered the Stimson formation of the Siccar Point group, a meter-scale cross-bedded aeolian sandstone unit that unconformably overlies the Mt. Sharp group.

Curiosity's exploration of the Glen Torridon region (Fig. 1-1) began on sol 2302 following an ~570 sol campaign at Vera Rubin ridge (VRR) (Fraeman et al., 2020). Orbital observations of this region of Mount Sharp using the High-Resolution Imaging Science Experiment (HiRISE), Context Camera (CTX), Thermal Emission Imaging System (THEMIS), and the Compact Reconnaissance Imaging Spectrometer for Mars (CRISM) revealed a topographic-low with strong phyllosilicate phases and a distinct reticulate texture (Anderson, 2010; Fraeman et al., 2016; Milliken et al., 2009). Compared to the overlying strata which appears to be sulfate-bearing, with little to no apparent clay mineral signatures, Glen Torridon (referred to as "phyllosilicate-bearing trough" in Anderson (2010), "phyllosilicate layers" in Milliken et al. (2010), and "phyllosilicate unit" or "PhU" in Fraeman et al. (2016)), was found to have spectral signatures consistent with Fe/Mg-bearing smectite clays (Fraeman et al., 2016). The transition from clay- to sulfate- bearing units is believed to chronicle a progression of climate change on ancient Mars associated with increasingly arid and acidic conditions (Bibring et al., 2006; Fraeman et al., 2016; Milliken et al., 2010).

Bedrock exposed within Glen Torridon is interpreted to be stratigraphically equivalent to, and an extension of, the Jura member first identified on VRR (Anderson, 2010; Fraeman et al., 2016). Within Glen Torridon, the Jura member forms a 6 m thick unit of resistant and recessively layered

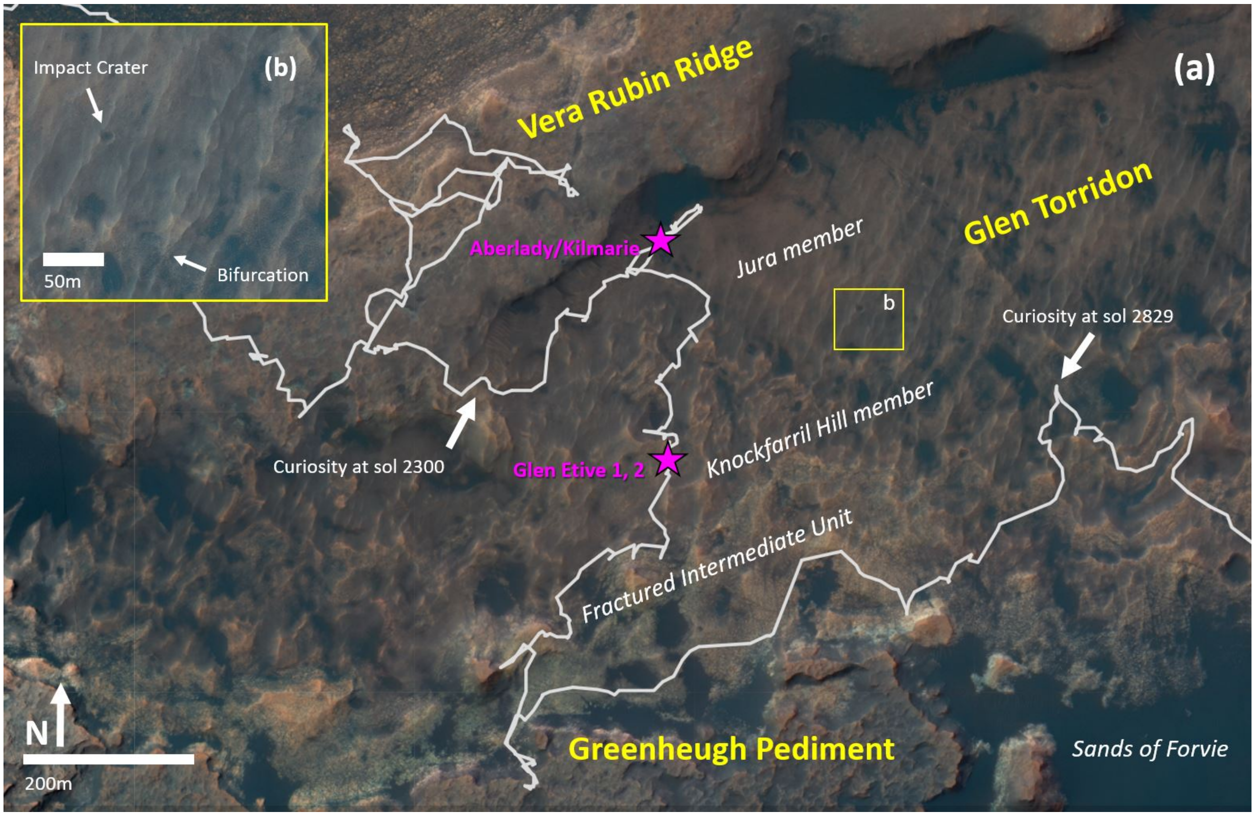

Figure 1-1 (a) Map of the Curiosity rover's traverse through Glen Torridon. (b) Slightly sinuous ridges oriented southwest to northeast are occasionally bifurcated or disrupted by small craters.

lacustrine mudstone enriched in K and Mg based on ChemCam measurements (Dehouck et al., 2019). A resistant sandstone unit known as the Knockfarril Hill member overlies the Jura member within Glen Torridon (Fox et al., 2020). The Knockfarril Hill member sandstones are easily distinguished by their decimeter-scale cross-bedding and resistance to weathering. The transition between the Jura and Knockfarril Hill members is interpreted to represent a transition from a low- to higher- energy depositional setting (Fox et al., 2020).

One of the most prominent features of Glen Torridon is the presence of decameter-long linear ridges interpreted as periodic bedrock ridges (Stack et al., 2019; this issue), which are prevalent in lower Glen Torridon. Presumed to be transverse to the prevailing wind direction and oriented towards the north-east, the PBRs are interpreted to be carved directly into the bedrock, though they are covered with pebble- to cobble- sized clasts. In this context, understanding the environment in which the Glen Torridon clasts formed may offer insight into the generation of PBRs and the erosion of the Knockfarril Hill member.

2 Data and Methods

2.1 Mastcam Clast Survey

Images captured by the MastCams are the basis for the study of clast size, shape and distribution. Systematic clast imaging has been conducted since Curiosity's landing in Gale crater (Yingst et al., 2010, 2013, 2016). Following nearly every drive completed by Curiosity, a "clast survey" image pair is taken of the ground near the rover with both the left and right eyes of the MastCams mounted atop the Remote Sensing Mast. The left Mastcam (M-34) has a 34 mm focal length and 18.4° x 15° effective field of view (Bell III et al., 2013), resulting in a 0.22 mrad/pixel resolution. The right Mastcam (M-100) has a 100 mm focal length, a 6.3° x 5.1° field of view, and a 0.074 mrad/pixel resolution. The standard subframe for clast survey images is 1152 x 1152 pixels, corresponding to a field of view of 14.4°x 14.4° for M-34 and 4.9° x 4.9° for M-100. The image scale is 0.62 mm/pixel and 0.21 mm/pixel for M-34 and M-100, respectively.

Clast survey images are taken at a consistent azimuth (120°) and elevation (-45°) in the coordinate frame of the rover, and most were acquired in the afternoon for consistent illumination in order to provide the best color contrast for distinguishing clasts from the sand substrate (Yingst et al., 2016).

2.2 MARDI

Images from the Mars Descent Imager (MARDI) are used to catalog qualitative morphological features of clasts (e.g. texture, angularity, erosional markers), the presence of bedrock, and clast dispersion. MARDI is a downward-pointing camera intended primarily for navigational use during MSL's entry, descent and landing (Malin et al., 2017). MARDI has since been used to systematically document the terrain covered by Curiosity since its landing in 2012 (Minitti et al., 2019). MARDI has a 70° x 52° field of view and an instantaneous field of view (iFOV) of 76 milliradians, ideal for long-range imaging. MARDI image quality decreases with spatial scale, but post-landing calibration has enabled the instrument to capture 1.5 mm resolution images of the surface directly below the rover (Malin et al., 2009). MARDI's orientation and proximity to the ground (70 mm) offers another dataset uniquely suited to clast imaging.

2.3 ChemCam

Elemental geochemistry obtained by the Chemistry and Camera (ChemCam) instrument is assessed in this study to determine compositional trends within clast types and between clast types and local bedrock. ChemCam uses Laser Induced Breakdown Spectroscopy (LIBS) to acquire major element abundances for SiO_2, TiO_2, Al_2O_3, $FeOT$, MgO, CaO, Na_2O and K_2O (Maurice et al., 2012). The LIBS technique involves striking a nearby target with a series of laser pulses to induce a short-lived plasma, from which emitted light produced by atom decay is spectrally analyzed (Maurice et al., 2012). ChemCam is particularly well-suited for clast analysis as it is sometimes able to target multiple small clasts within a single raster and without the need for contact science. In conjunction with LIBS analysis, ChemCam captures submillimeter resolution images of targets using its Remote Micro-Imager (RMI). RMI has a field of view of 20 mrad and a pixel scale of 19.6 μrad/pixel (Maurice et al., 2012). A total of 28 RMI images were used to characterize clast texture and grain size.

2.4 Analysis of Clast Characteristics

Shape and size clast measurements were obtained by analyzing 64 Mastcam clast survey image pairs captured between sols 2302 and 2593. For unbiased clast sampling, 50 x 50 and 10 x 10 grids were superimposed onto the M-34 and M-100 images, respectively. Any clasts within a given cell in the grid were eligible to be sampled and digitally outlined in ImageJ. Following the methods of

Yingst et al. (2016), we measured clast major and minor axis, sphericity, solidity, and roundness. Sphericity, f, approximates the resemblance of a particle to a sphere from its two-dimensional projection (Riley, 1941). Sphericity is a function of the largest inscribing circle diameter, d_i, and the smallest circumscribing circle diameter, d_c, of a particle given by;

$$f = \sqrt{d_i / d_c}$$

Solidity, S, is a measurement of the concavity of a clast, defined as the ratio of clast area, A, to convex hull area, Ac (Olson, 2013). As the clast becomes smoother and more rounded, the area of the clast and that of its convex hull area will converge to 1. Since surface roughness and protrusions strongly affect the value of Ac, solidity can be used as a proxy for surface texture.

$$S = A / A_c$$

Roundness is a measure of corner sharpness. Roundness classes defined by Powers (1953) include very-angular, angular, sub-angular, sub-rounded, rounded and well-rounded. Clast roundness in this work is determined by visual assessment.

The accuracy of morphological measurements is highly dependent on image resolution and surface illumination. For the purposes of this study's analysis, the resolution limits on major axis (minimum major axis of 12 mm for M-34 and 4.2 mm for M-100) and shape parameters (minimum major axis of 60 mm for M-34) defined by Yingst et al. (2016) are adopted, with the exception of the minimum major axis limit for shape resolution on M-100 images, which is reduced from 21 mm to 20 mm to incorporate more clasts given the quantity of small pebbles in the region. Any clasts measured below these threshold values were marked and bundled as "fines".

Error in clast morphology measurements is predominantly caused by measurement error and the use of a two-dimensional projection to estimate the parameters of a three-dimensional shape (Yingst et al., 2010), an issue potentially exacerbated by the fact that the fixed orientation of the Mastcam for clast survey images means clasts deposited along slopes are angled differently than those on level ground. Although we acknowledge several potential sources of error, Riley (1941) and Cailleux (1947) show this error to be less than 10% for pebble- to cobble- sized clasts that are sub-angular to well rounded, which is the case for the vast majority of clasts observed in this dataset. We consider this error to be within an acceptable range.

Clast lithology, including texture and grain-size, were assessed qualitatively using Mastcam clast survey images, MARDI images, and finally ChemCam RMI captures where available.

2.5 Approach to Clast and Outcrop Geochemistry

ChemCam targets of in-place bedrock outcrops analyzed between sols 2225 to 2579 were identified as either Jura or Knockfarril Hill member based on their stratigraphic position (elevation) and on a visual assessment of lithology: Jura member is comprised of laminated mudstones; Knockfarril Hill is typically comprised of coarse-grained sandstones. To visualize the major geochemical trends of both members, density contour plots were generated from the bedrock target data. Density contours are two-dimensional histograms used to plot bivariate distributions, which are smoothed using kernel density estimation for this analysis. The contour lines connect points with the same probability density values and are adjusted according to the number of targets per unit. The major element oxide wt.% is averaged across a target in order to express the effective bulk composition of the target rock. Clasts compositions were then plotted together with in-situ Jura and Knockfarril Hill member bedrock targets in order to compare clast composition with local bedrock. Since composition can vary significantly from raster point to raster point for coarse-grained rocks, or when rasters cross multiple clasts, plots show the composition of individual raster points rather than target averages.

3 Results

3.1 Clast types

Based on analysis of shape, size, and texture, eight primary clast types were identified (Fig. 3-1, 3-2) within Glen Torridon. Features of three-dimensional shapes can be lost in two-dimensional projections, but unique and easily distinguishable three-dimensional characteristics such as facets and laminations were recorded by visual assessment. Clast types 1-3 are classified predominantly using such qualitative evaluations. The remaining clast types (4-8) have distinct and quantifiable shape and size characteristics (Table 3.1, Fig. 3-3). Only clasts with similar properties observed over three or more sols were consolidated into types.

The lithology of all the clast types observed in Glen Torridon is interpreted to be sedimentary. These clast types commonly exhibit laminations, smooth surface textures, and fine grain sizes down to RMI scale images. These features are similar to that of in-place Jura and Knockfarril Hill member bedrock, as well as other Murray formation rocks observed along Curiosity's traverse through Gale crater. No clasts observed in this study displayed porphyritic textures. That said, many of the clasts in Glen Torridon are coated with a layer of dust that obscures color and grain size, complicating assessments and comparisons of lithology across and among clast types and bedrock.

Table 3.1: Average shape and size parameters of clast types 1-8

Clast Type	*Major Axis (mm)*	*AR*	*Sphericity*	*Solidity*	*Roundness*
Type 1	15.0	1.86	0. 71	0.88	A – SR
Type 2	23.0	1.68	0.75	0.94	SR
Type 3	22.7	1.56	0.77	0.94	SR – R
Type 4	< 4	-	-	-	SR – WR
Type 5	10.9	1.46	-	-	R – WR
Type 6	14.0	2.25	0.66	0.91	A – SR
Type 7	25.3	1.42	0.80	0.94	SR – R
Type 8	10.9	1.43	-	-	A – SA

3.1.1 Type 1

Type 1 clasts (Fig. 3-1a) are angular to sub-rounded, with an average clast diameter of 15 mm (Table 3.1). This clast type is platy and elongate, leading to high aspect ratios. Type 1's have rough, unpolished surfaces and often appear laminated. These clasts are fine-grained. Type 1 clasts are relatively rare, and exist primarily in the northern region of Glen Torridon at low elevations. This type occurs commonly on or near bedrock interpreted to be in-place based on the extent (at least several meters), continuity of exposure, and uniformity of lithology.

3.1.2 Type 2

Type 2 clasts (Fig. 3-1c, 3-1d) are sub-rounded and have an average clast diameter of 23 mm (Table 3.1). This type is distinguished by its rectilinear shape, with multiple flat faces oriented at approximately 90° angles from one another. Type 2 clasts are smooth textured and fine-grained, with some clasts exhibiting lamination. These clasts range from matte to polished in appearance. Type 2's are well-distributed along the traverse through Glen Torridon, but are especially common near bedrock outcrops.

3.1.3 Type 3

Type 3 clasts (Fig. 3-1e, 3-1f) are sub-rounded to rounded and are one of the largest clast types observed, with an average diameter of 22.7 mm (Table 3.1). This clast population is characterized by the presence of a facet, a convexly-curved face that terminates at a sharp edge known as a keel. Type 3 clasts contain one or more facets that tend to meet at obtuse angles to form single-edged einkanter or pyramidal dreikanter shapes. This type is fine-grained, smooth textured, and often polished. Most Type 3 clasts are marked with pits, flutes and grooves. Type 3 clasts are particularly abundant near the periodic bedrock ridges throughout Glen Torridon.

3.1.4 Type 4

Type 4 clasts (Fig. 3-1b) are sub-rounded to well-rounded, and the smallest clasts observed in this study. The diameter of these clasts is generally 4 mm or less. Since the clast size approached the resolution limits of the images, additional size and shape statistics were not gathered for this type. Type 4 clasts are smooth textured and have a matte surface appearance. This clast type is abundant throughout Glen Torridon.

3.1.5 Type 5

Type 5 clasts (Fig. 3-2a) are rounded to well-rounded with an average diameter of 10.9 mm (Table 3.1). Clasts of this type are highly spherical, and are often found as ovular rocks with one flat face. Type 5 clasts are smooth textured and fine-grained. These clasts are generally well-polished. Type

5's appear in well-sorted patches near the base or tail-ends of ridge-slopes throughout Glen Torridon.

3.1.6 Type 6

Type 6 clasts (Fig. 3-2b) are angular to sub-rounded. These clasts have an average diameter of 14 mm (Table 3.1). This clast type is distinctly elongate, often appearing to have at least one heavily tapered end. As a result, Type 6 clasts have the highest aspect ratios of all the clast types outlined in this study. These clasts are smooth textured and fine-grained, and are occasionally observed with laminations and varying degrees of polish. This type is found predominantly in the troughs between ridge-crests.

3.1.7 Type 7

Type 7 clasts (Fig. 3-2c, 3-2e) are sub-rounded to rounded. These are the largest clasts in Glen Torridon with an average diameter of 25.3 mm (Table 3.1). Type 7 clasts are highly spherical and often appear dome-shaped. This clast type is smooth-textured, fine-grained, and very well-polished. Many Type 7 clasts exhibit lamination. These clasts occur throughout the traverse, but are most densely near PBRs and other ridges.

3.1.8 Type 8

Type 8 clasts (Fig. 3-2d) are angular to sub-angular, with an average diameter of 10.9 mm (Table 3.1). This clast type comes in a variety of shapes, but has the lowest average aspect ratio (AR = 1.4). Type 8 clasts can be rough or smooth textured, and depending on the texture, may appear medium or fine-grained. These clasts are generally unpolished and well-laminated. Type 8 clasts are abundant throughout Glen Torridon.

3.2 Distribution of Clast Types

The spatial distribution of clast types in the Glen Torridon region is mapped in Figure 3-4. As noted in Section 3.1, Type 1 clasts are predominantly located in northern Glen Torridon at low elevations, in an area of in-place bedrock exposure just south of the Vera Rubin ridge. Type 1 clasts rarely occur near the PBRs, which are not particularly common in this area of Glen Torridon. Type 2 and 3 clasts appear frequently near PBRs and other ridges, including those oriented discordant to the northeast to southwest bearing of the PBRs. Type 7 clasts are rare, but appear to be densely packed near PBRs and other ridges. Clast Types 4, 5, 6, and 8 are observed throughout Curiosity's traverse of Glen Torridon, with no apparent bias towards any locality of Glen Torridon or any of its geologic features. No significant up-section trends in clast type distribution are observed.

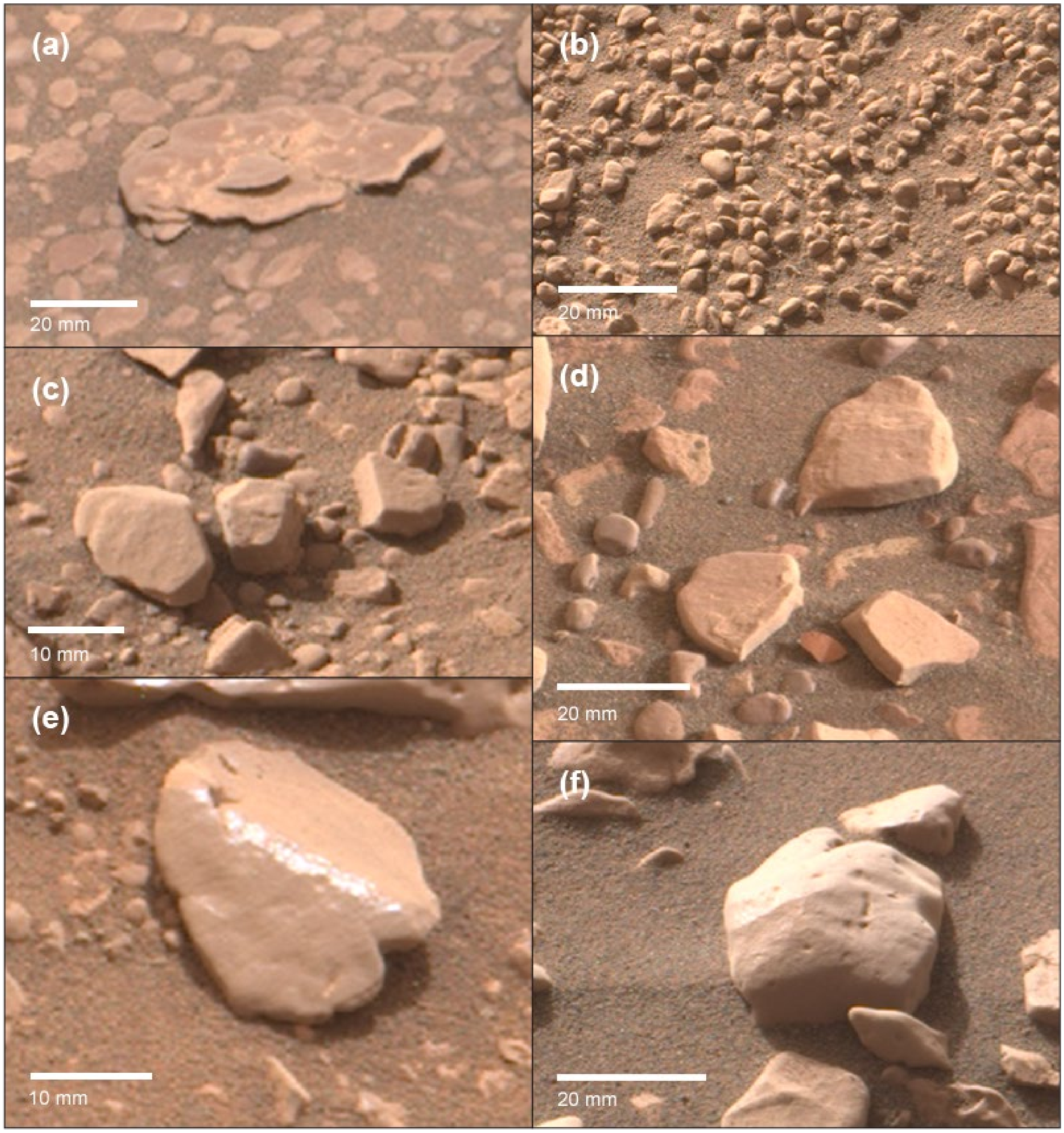

Figure 3-1 M-100 images of clast types 1-4. (a) Type 1 clast, sol 2357, (b) Type 4 clasts, sol 2577, (c) Type 2 clasts which appear to have broken apart in-situ, sol 2480, (d) Type 2 clasts, sol 2320, (e) Type 3 clast, sol 2306, (f) Type 3 clast exhibiting slope retreat towards central keen, sol 2568.

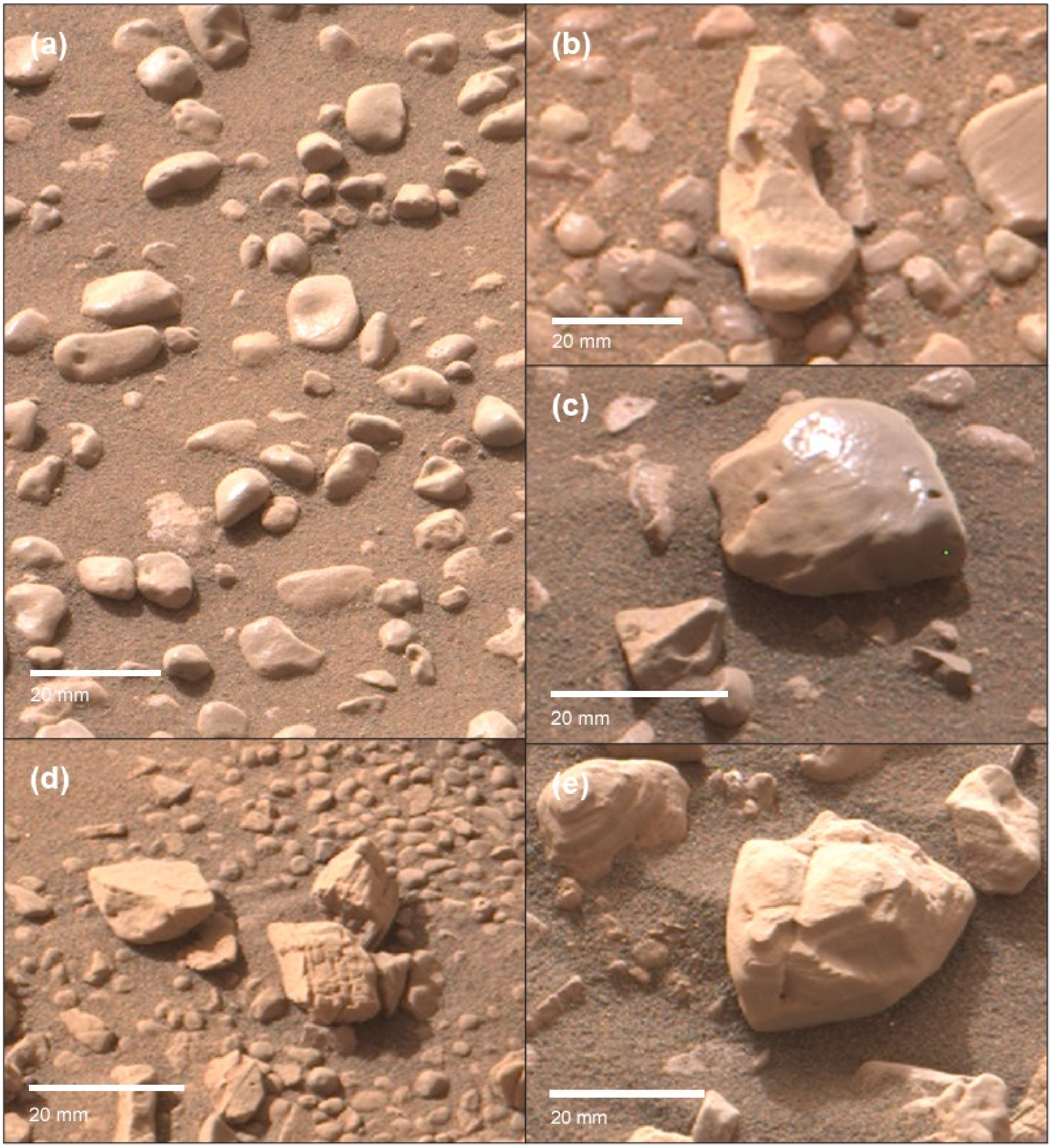

Figure 3-2: M-100 images of clast types 5-8, (a) Type 5 clasts, sol 2466, (b) Type 6 clast, sol 2304, (c) Type 7 clast with polished surface, sol 2477, (d) Type 8 clasts, sol 2480, (e) Type 7 clast with clear lamination, sol 2475

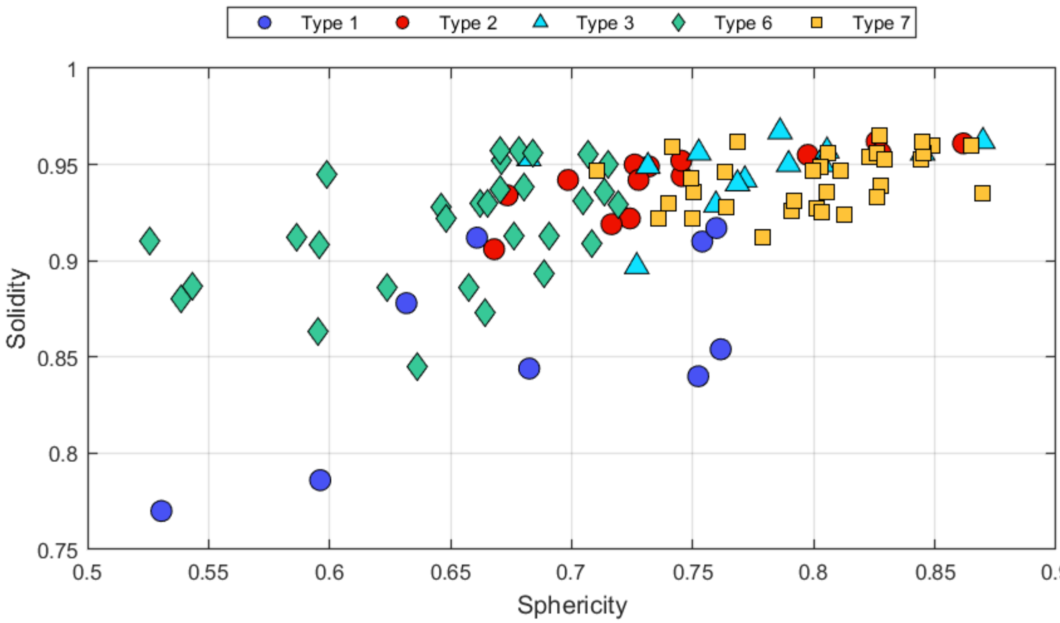

Figure 3-3 Plot of clast types as a function of solidity and sphericity. Given shape parameter resolution limit, only clasts with a major axis > 20 mm are plotted.

3.3 Proximity to Periodic Bedrock Ridges

Three PBRs were identified along the rover traverse with Mastcam clast survey images taken within 15 meters of the PBR crest. PBR 1 (sols 2302-2309) is located near the southern rim of the Vera Rubin ridge in the Jura member. The rover approaches the PBR 1 crest to the south of a Knockfarril Hill member outcrop which caps the ridge. PBR 2 (also known as Teal ridge, sols 2436-2447) is near the transition between the Jura and Knockfarril Hill member transition. The rover approaches PBR 2 where it terminates at a large Knockfarril Hill member outcrop. PBR 3 (sols 2586-2590) is in the Knockfarril Hill member near the transition to the Glasgow member.

Trends in shape and size parameters along the ridge profile are illustrated in Figure 3-5. In general, sphericity and solidity are minimized at the ridgecrest, indicating clasts are rough and non-spherical. Sphericity approaches a maximum within 5 to 10 meters of the ridgecrest in both the NW/SE directions. Solidity is maximized in the SE direction. PBR 2 deviates from these patterns, showing an overall increase in sphericity and solidity towards the crest. This may be the result of localized air movements produced by the high standing Knockfarril Hill member outcrop. Trends in size are less consistent. Major axis is maximized at the crest of PBR 1, but minimized at the crest of PBR 3. At PBR 2, major axis is higher than average at the crest, but increases to its maximum value approximately 10 meters to the northeast of the ridgecrest. Larger clasts at or near the crests of PBRs 1 and 2 is likely due to the presence of coherent bedrock caps. Along the PBR flanks, clasts are also found to be more angular and poorly sorted, or in small densely-packed patches. At the troughs, clasts are rounded, well-sorted and more deeply embedded in the sand matrix.

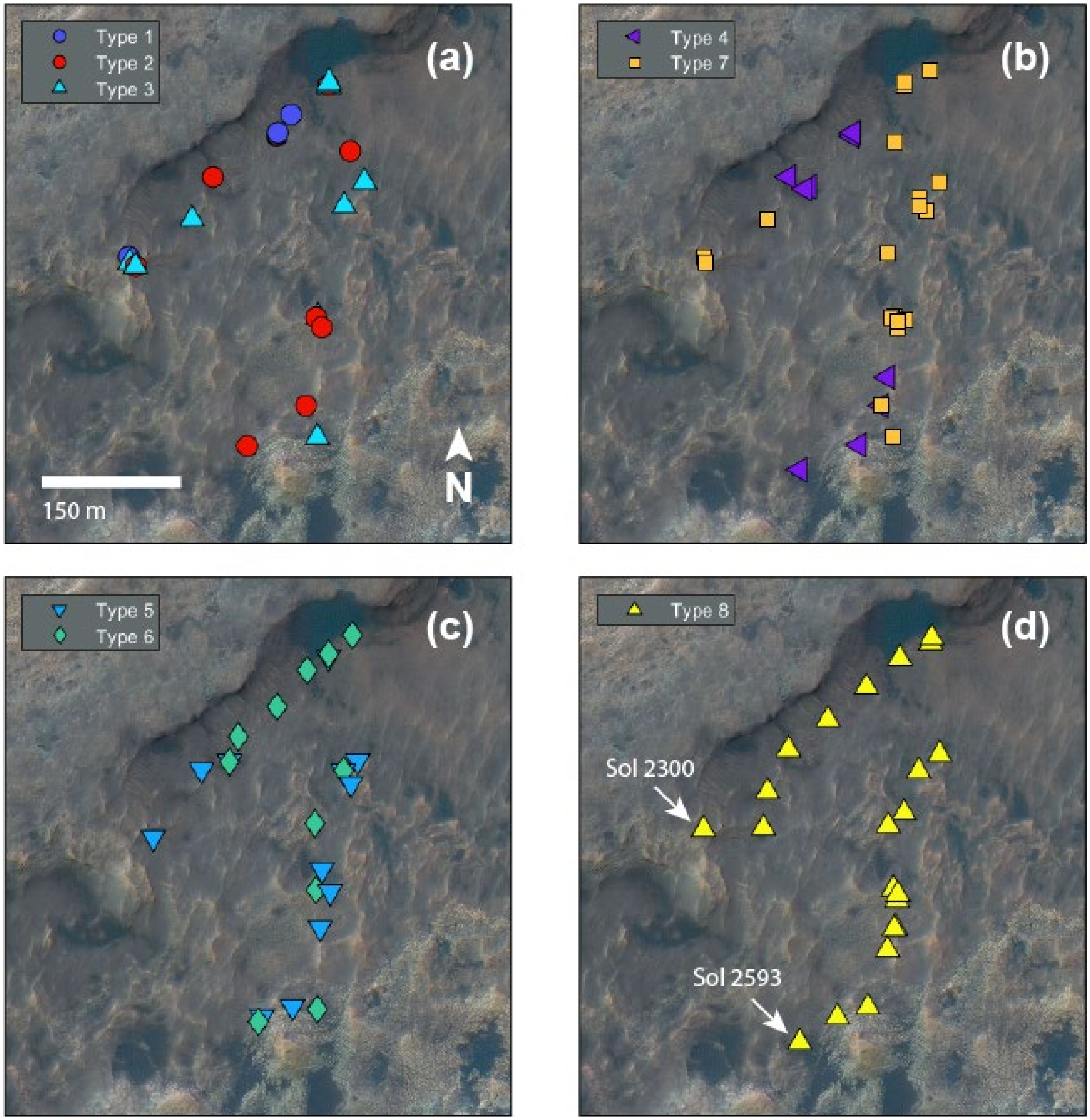

Figure 3-4: Spatial distribution of clast types. Points in plots A and B represent locations where clast types represent ≥5% of the sampled population, since these types occur infrequently. Points in plots C and D represent locations where clast types represent ≥30% of the sampled population. Type 4 clasts are mostly under the major axis resolution limit and thus appear localized, but in fact these clasts are abundant along the traverse troughs.

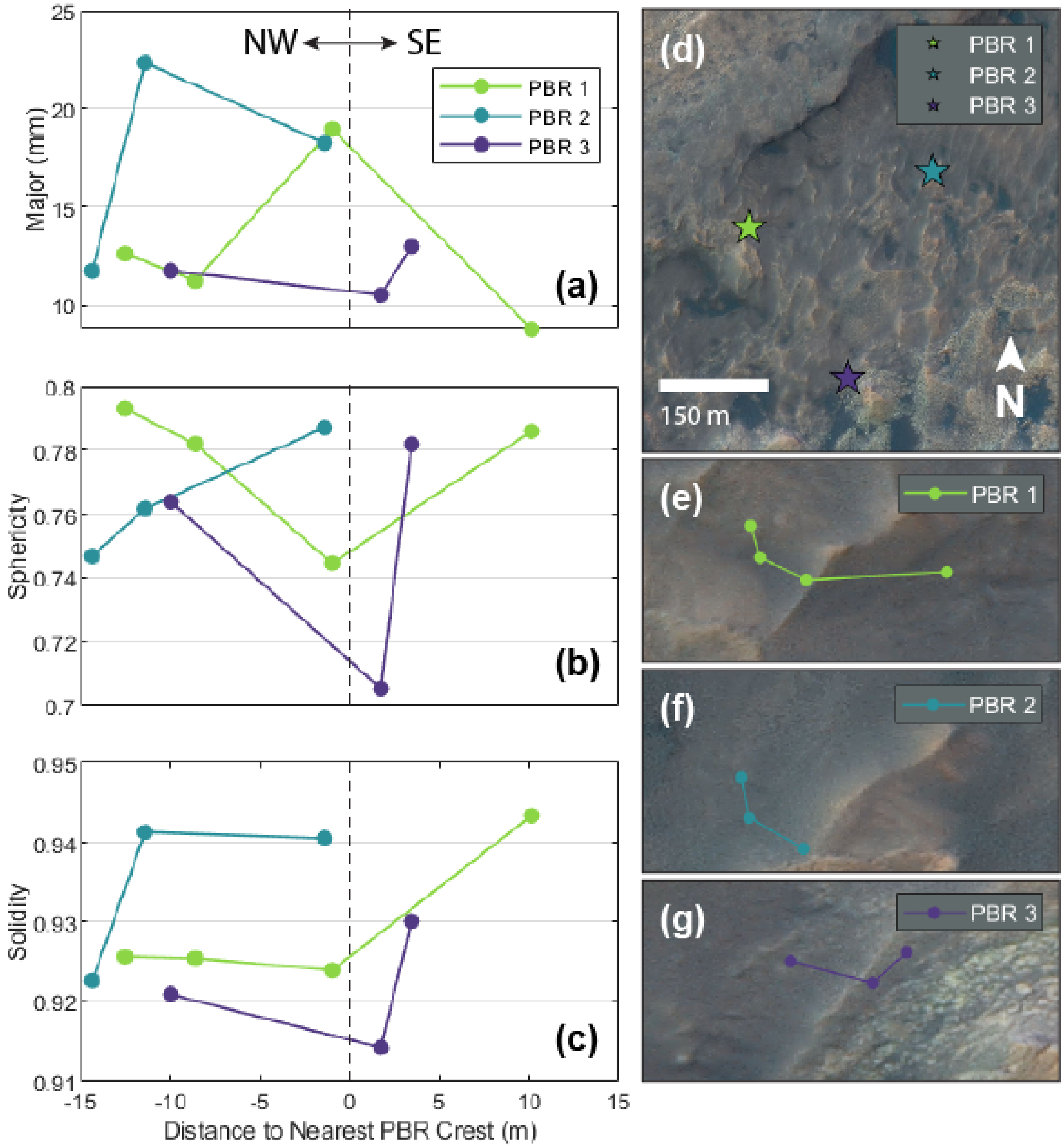

Figure 3-5: (a)-(c) Average size and shape measurements of clasts imaged at each rover position along the PBR with respect to approximate distance from the PBR crest. (a) Map of three PBR locations in Glen Torridon. (e) -(g) Rover positions with respect to each PBR.

3.4 Geochemistry

Major element abundances measured by the ChemCam instrument show clast composition is closely correlated with nearby corresponding bedrock composition (Fig. 3-6), consistent with the findings of Dehouck et al. (2019). Over 63% of the ChemCam raster points on clasts are enriched

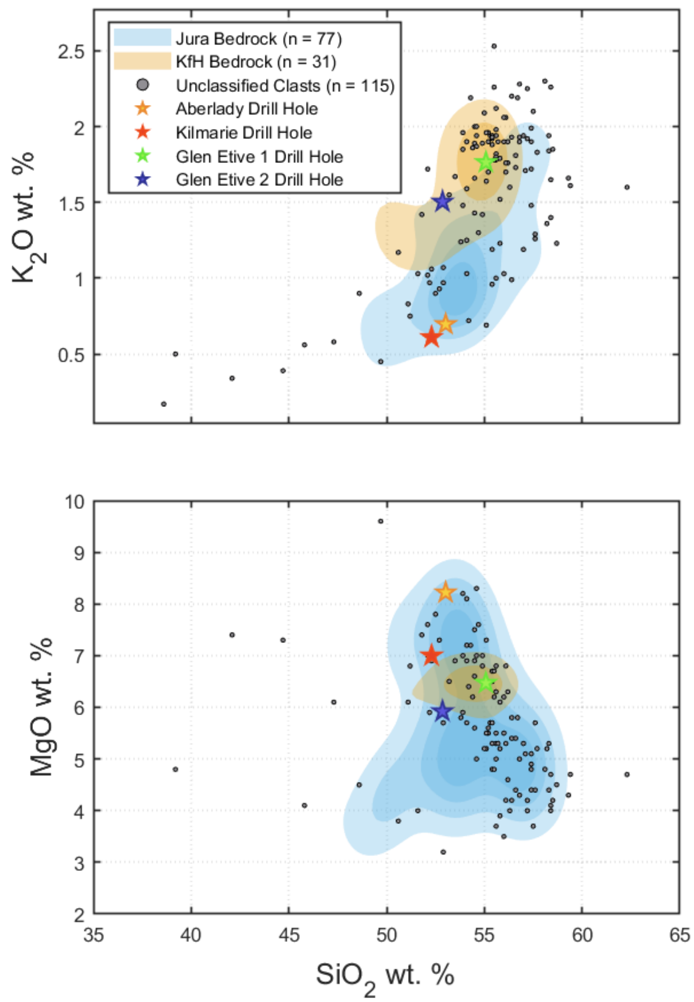

Figure 3-6: Density contours of Jura and Knockfarril Hill members for select major element oxides, averaged by target. The Knockfarril Hill contour is elevated in K_2O and depleted in MgO compared to Jura. The average compositions of drill targets, represented by stars, reflect this trend. Aberlady and Kilmarie samples were taken from Jura bedrock, while Glen Etive samples 1 and 2 are taken from Knockfarril Hill.

in K_2O (> 1.5 wt. %), suggesting a majority of clasts in Glen Torridon are sourced from the Knockfarril Hill member, which is enriched in K_2O relative to the underlying Jura member (Dehouck et al., 2019). Glen Torridon clasts depleted in K_2O tend to display an enrichment in MgO, a characteristic of the Jura member bedrock. These compositional trends are reflected in the Glen Torridon drill targets, which sample both the Jura member bedrock (targets Aberlady and Kilmarie) and the Knockfarril Hill member bedrock (targets Glen Etive 1 and Glen Etive 2). These results together strongly indicate that the provenance of the clasts analyzed in this study is relatively local and primarily within Glen Torridon.

4 Discussion

4.1 Aeolian Abrasion

Aeolian processes are well-established as the dominant drivers of surface modification on modern Mars, but low gravity and a thin atmosphere necessitate strong winds to initiate grain transport (R. Greeley, 1984; R. Greeley et al., 1992, 2001, p. 2; Wells & Zimbelman, 1997). Saltating sand, rather than bedload transport, facilitate wind abrasion on the martian surface (Baker et al., 2017; Sullivan & Kok, 2017). Rocks formed by the abrasive action of sand are known as ventifacts (Mary Bourke & Viles, 2007; Cooke et al., 1993; Whitney & Dietrich, 1973), which are characterized by convexly shaped impact surfaces (facets) that meet at a sharp edge called a keel. Facets and keels are often oriented perpendicular to the prevailing wind-direction, but winds approaching from multiple directions and clast overturning can lead to the development of three or more facets on a single clast (Durand & Bourquin, 2013). Sandblasting produces a variety of other features at the facet scale, including pits, flutes and grooves (Mary Bourke & Viles, 2007; Cooke et al., 1993; Whitney & Dietrich, 1973).

Ventifact evolution is controlled by the initial clast shape and texture (Durand & Bourquin, 2013; King, 1949; Laity & Bridges, 2009; Whitney & Dietrich, 1973). Existing faces will develop into convexly sloping facets, and surface irregularities will expand into pits, flutes or grooves. Surfaces on an individual clast may also appear rough, matte or polished – depending on the degree and nature of erosion. Sandblasted ventifacts will be rougher, whereas ventifacts abraded by dust may develop a polish.

Abrasion in fluvial flows is also capable of producing the features and morphology typically associated with ventifacts (Mary Bourke & Viles, 2007; Durand & Bourquin, 2013). Limited research has been conducted to distinguish between features common to fluvial and aeolian erosion, however, these features are generally believed to develop on mega-clasts and bedrock in a fluvial setting, rather than the granule- to cobble-sized clasts common in Glen Torridon (Mary Bourke & Viles, 2007).

Signs of extensive aeolian abrasion have been observed at the Pathfinder, Spirit, and Opportunity landing sites, as well as in Gale crater (Bridges et al., 1999, 2014; Golombek et al., 2006; Ronald Greeley et al., 2002; McCauley et al., 1979; Sullivan et al., 2005; Thomson et al., 2008). Rocks in Glen Torridon appear to be modified to a much lesser degree, but evidence of wind-abrasion is still abundant. Type 3 clasts are defined by the presence of the convex facet and keel typical of the ventifact. Critically, Figure 4-1 reveals multiple Type 3 clasts with keels oriented in the same direction, suggesting they were modified by the same wind. This helps to rule out fluvial abrasion as the source of facets and other features (i.e. pits, grooves, flutes) for at least some of the clasts in Glen Torridon, since fluvially transported clasts are unlikely to be found in such a precise configuration. Pits and shallow grooves are visible on clasts from the cobble- down to granule-scale. Many clasts also exhibit surface polish (ex: Fig 3-1e, 3-2c). Bedrock features offer further confirmation of aeolian action in Glen Torridon: Jura member bedrock is often polished, and Knockfarril Hill member bedrock outcrops are etched, a consequence of differential erosion. Establishing the presence and extent of aeolian abrasion in Glen Torridon enables us to better

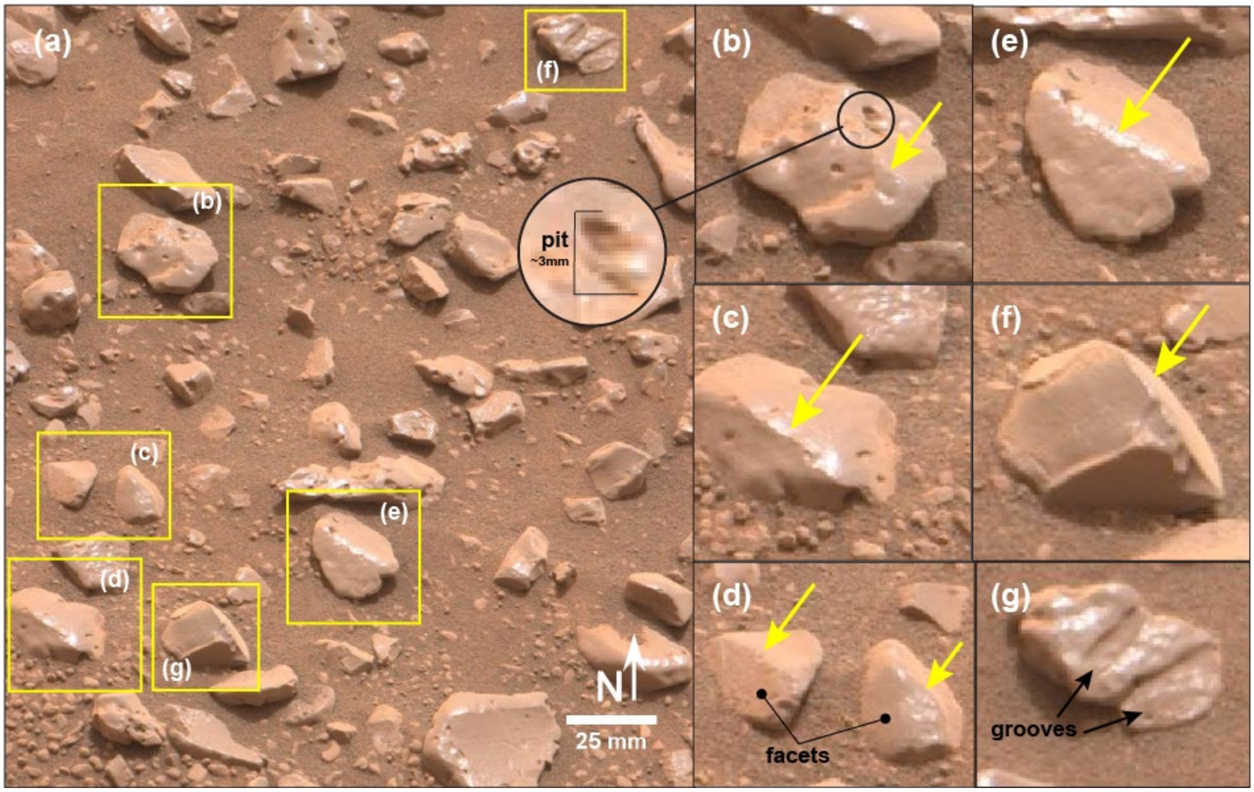

Figure 4-1: Features of aeolian abrasion on Glen Torridon clasts from sol 2306. Yellow arrows point to keels, which are oriented in the same direction for multiple clasts.

distinguish between features of primary processes and recent modification preserved on the clasts in this study.

4.2 Source of the Glen Torridon Clasts

We examine four possible mechanisms by which the clasts in Glen Torridon could have been formed: (1) impact cratering, (2) fluvial or debris flow, (3) glacial erosion, and (3) in-situ bedrock degradation.

4.2.1 Impact cratering

Impacts can produce clasts with a variety of shapes, textures and sizes. Diagnostic features of impact ejecta blocks include shocked minerals, impact melts, melt-brecciation, shatter textures, and shatter cones (Newsom et al., 2015; Osinski & Pierazzo, 2012). Shocked minerals may be expressed as linear striations at the clast-scale (Osinski & Pierazzo, 2012). Clasts that have experienced shock may also exhbit shatter textures and shatter cones, macroscopic features that appear as subparallel lineations and conical striations (Osinski & Pierazzo, 2012). At higher pressures, clasts can undergo partial or complete melting, resulting in vesicular and porphyritic textures (Newsom et al., 2015; Spray et al., 2010; Therriault et al., 2002). Melts may also incorporate local fragments to form impact melt breccias, or consolidate into clasts known as spherules (Glass, 1990; McCall, 2001). Spherules are small, smooth and highly-spherical glass particles. Newsom et al. (2015) identified potential spherules on sol 291 that appear similar in size and shape to some Type 4 clasts. Though spherules are typically highly reflective on account of their composition, the dull appearance of many Type 4 clasts may be the consequence of thick dust coatings. Type 4 clasts could alternatively be interpreted as lapilli, a type of proximal ejecta that accrete ash and glass as they fall back to the surface (Newsom et al., 2015). Lapilli have rough, porous surfaces which permit thicker layers of dust to accumulate, contributing to their lackluster appearance. However, with the possible exception of Type 4 clasts, little evidence exists of impactite features on Glen Torridon clasts. While shock features such as shatter cones may be overprinted by fluvial or erosional processes, there are no observations of brecciation or textures associated with melting in Glen Torridon.

The uniformity of clast lithology and composition is also inconsistent with an impact formation interpretation. If Glen Torridon clasts are in fact an accumulation of ejecta from impacts across Gale crater and beyond, we would expect far greater lithochemical diversity. As described in Section 3.4, nearly all clasts analyzed in this study are lithologically and compositionally similar to each other, and in-family with in-place observations of Jura or Knockfarril Hill member bedrock. Impact ejecta may constitute of small portion of the clasts in Glen Torridon, but impact events are unlikely to be the primary driver of clast formation in the region.

4.2.2 Fluvial or debris flow

Fluvial or debris flows are capable of transporting and depositing large quantities of gravel-, pebble-, and cobble-sized clasts. Debris flows are able to transport granule- to cobble- sized clasts (Whipple & Dunne, 1992), and studies of the Peace Vallis alluvial fan at the crater rim indicate fluvial flows can support clasts up to 10 cm in diameter (Cousin et al., 2021; Sautter et al., 2014, 2015), significantly larger than the clasts observed in Glen Torridon. Fluvial or debris flow transport could explain the quantities of rounded clasts found throughout Glen Torridon, specifically the Type 4 and 5 varieties, which are characteristically rounded to well-rounded. Assuming the clasts of Glen Torridon all derive from a common source and erosional pathway, angular deposits can be accounted for in this model by shorter transport distances.

Unlike in debris flows, abrasion in fluvial flows is also capable of producing pits, grooves, flutes, facets and polish (Mary Bourke & Viles, 2007; Durand & Bourquin, 2013). However, it is unclear to what extent aeolian processes may have overprinted on features of fluvial transport in Glen Torridon. Laboratory studies by Bourke et al. (2007) suggest features distinct to fluvial processes (i.e. percussion terminations) are among the first to be eroded away by wind abrasion. If this is the case in Glen Torridon, it will be difficult to distinguish whether such features are fluvial or aeolian in origin.

If the Glen Torridon clasts were transported to their current location by fluvial and debris flows entraining sediments from the upper slopes of Mount Sharp, the crater rim, or terrain outside Gale, lithological and geochemical diversity, like that observed on Bradbury Rise (Cousin et al., 2021) would be expected. The uniformity in clast lithology and composition does not support a fluvial or debris flow origin of the clasts found within Glen Torridon.

The Glasgow member and the Greenheugh pediment south of Glen Torridon towards Mount Sharp are distinct both lithologically and in composition. The Glasgow member, in particular, is depleted in K_2O and MgO compared to the mean Jura and Knockfarril Hill member compositions (O'Connell-Cooper et al., 2021). It is unlikely that Glen Torridon clasts are sourced from either of these units. While Jura member present on Vera Rubin may be a source for clasts in Glen Torridon, only about 30% of Glen Torridon clasts observed in this study are interpreted as Jura member. Fluvial and debris flows from VRR would not account for the majority of clasts in the region.

4.2.3 Glacial erosion

Glacial processes enable pebble- to boulder-sized clast formation. Depending on the thermal regime and transport path through the glacier, glacial clasts can range from sub-angular to sub-rounded, and exhibit faceted or "flat-iron" morphologies (Atkins, 2003, 2004; Benn & Evans, 2014; Boulton, 1978; Sharp, 1982). Flat-iron clasts are wedge-like and occasionally wear in an asymmetrical fashion: rounded at the stoss-side and angular at the lee-side. The most commonly cited feature of glacial clasts is linear striae, which can be several centimeters deep at the clast-scale (Atkins, 2003). Striae are known to form near parallel to the long-axis direction and grow deeper in proportion to the size of the clast. The presence of both facets and striae on a clast is considered a strong indicator of glacial transport (Atkins, 2003, 2004).

Glen Torridon clasts present weak signatures of glacial erosion. Type 2 and 3 clasts are characterized by faces that may be interpreted as glacial facets, but these clasts differ in form from glacial clasts. Type 2 clasts are rectilinear rather than wedge-shaped, and the majority of Type 3 clasts have convex faces, atypical of clasts formed under glacial influence. Deep channels interpreted as aeolian flutes (Fig. 4-1g) may instead be interpreted as striae. However, in the case of Figure 4-1g, the channels are not oriented along the long axis of the clast, and are considerably deep given the size of the clast itself. It is possible that this clast and others like it in Glen Torridon eroded from larger, striaed boulders. Channels such as the ones illustrated in Figure 4-1g are rare in both the clasts and bedrock of Glen Torridon. If shallow glacial striae had existed in Glen Torridon, it is likely that secondary processes such as aeolian and fluvial abrasion have erased them. As with the aforementioned clast formation processes, glacial deposits are expected to have a degree of lithochemical diversity which is not observed in Glen Torridon.

4.2.4 In-situ bedrock degradation

Another pathway capable of producing the quantity of clasts in Glen Torridon is through the breakdown of local bedrock into cobbles, pebbles and granules. In this scenario, clasts detach from bedrock along pre-existing fractures and bedding planes. Cracks are known to form and expand by mechanisms such as frost heave, freeze-thaw, diurnal thermal fluctuations, crystal growth and

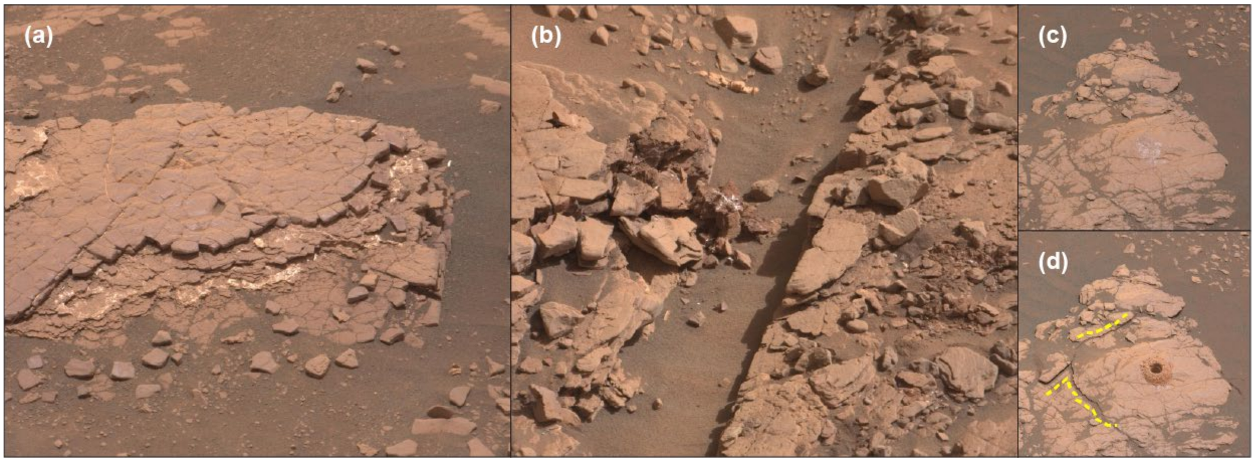

Figure 4-2: (a) Woodland Bay outrcrop (KfH), sol 2359, (b) Risk target (KfH), sol 2501, (c) Aberlady outcrop (Jura) before drilling, sol 2368, (d) Aberlady outcrop after drilling, sol 2370, revealing breakage along cracks and bedding planes (traced in yellow), possible precursor to a Type 1 clast.

dirt cracking (Bloom, 1978; Mary Bourke & Viles, 2007; Ollier, 1965). Fractures can produce clasts with varying shapes and degrees of roundness, and lithology strongly controls the pattern and occurrence of fractures formed by these breakdown processes (Bourke & Viles, 2007).

The Jura and Knockfarril Hill members of Glen Torridon both display a tendency to fracture in accordance with this model. The Woodland Bay outcrop of the Jura member has interbedded thick and thin layers separated by fracture fill material (Fig. 4-2a). Clasts in the immediate vicinity of Woodland Bay, identified as Type 2 clasts, exhibit similar morphologies as the blocks that make up bedding layers of this outcrop. Similarly, outcrops of the Knockfarril Hill member are heavily bedded and appear to fracture along fracture fills as well as internally. Near the Risk target in the Knockfarril Hill member are clasts which appear to have recently detached from the bedrock (Fig. 4-2b), including blocky Type 2 clasts and angular clasts reminiscent of Type 7 and 8 clasts ,which may have formed as the result of internal fracturing. The presence of smectite clay-minerals in Glen Torridon may contribute to the friability of both members. Smectite clays are a type of phyllosilicate clay susceptible to swelling when exposed to water. The smectites are composed of alternating layers of tetrahedral silicate and octahedral aluminum sheets. Cations in the interlayers readily absorb water, causing the clay to expand in proportion to the water available. The hydration and dehydration of clay minerals in Glen Torridon could have contributed to the tendency of the Jura and Knockfarril Hill members to break and form clasts.

The strongest support for this process is the similarity in lithology and composition between the Glen Torridon clasts and in-place bedrock exposures of the Jura and Knockfarril Hill members throughout Glen Torridon. Bedrock degradation would be expected to preferentially decay the overlying Knockfarril Hill member until Jura member bedrock is exposed, which is also supported by the prevalence of Knockfarril Hill-like clasts present throughout Glen Torridon.

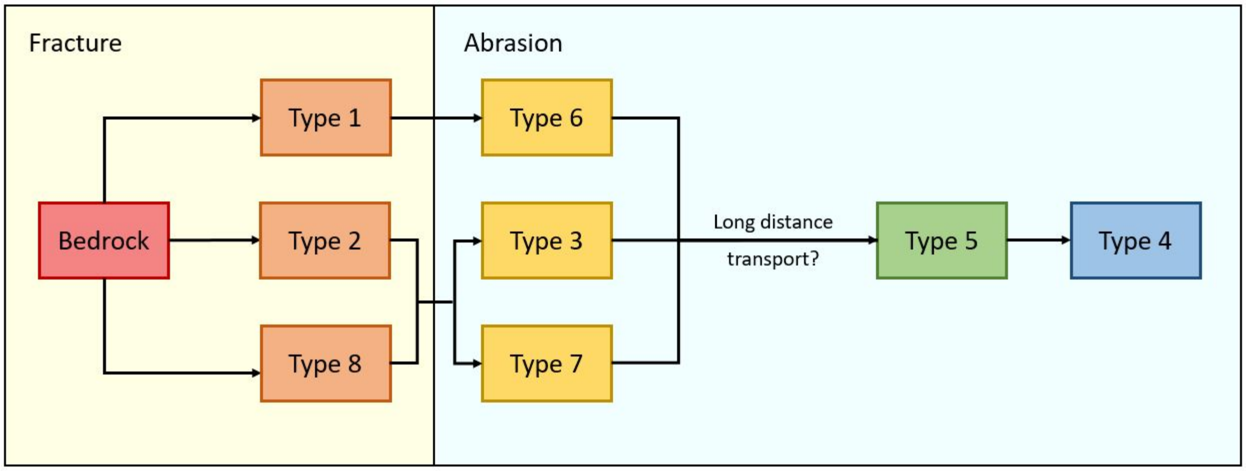

Figure 4-3: Proposed clast lifecycle. Rounding, solidity and circularity increase from left to right

4.3 Erosional Continuum for the Glen Torridon clasts

The strong similarities in clast morphology, lithology, and composition to the local bedrock points to in-situ bedrock degradation as the most likely source of the clasts in Glen Torridon. Outcrops such as Woodland Bay, North Berwick and the Glen Etive drill site illustrate clasts in the process of loosening from the bedrock along fracture fills, laminations and recessive bands. Clasts near bedrock outcrops are generally more angular, blocky or platy – reflecting the shapes of polygonal cracking within the bedrock itself – while lacking prominent surface features like pits, flutes and facets. The absence of these erosional features in "fresh" clasts supports an interpretation of secondary modification by aeolian processes. As clasts migrate away from bedrock and are exposed to impacting dust and sand particles, ventifact features are allowed to develop. Many clasts also exhibit lamination, a distinctive feature of Jura and Knockfarril Hill member bedrock.

Unlike the fluvial, debris flow, glacial erosion, and impact cratering models, bedrock degradation explains the agreement between clast lithology and composition to the local bedrock, as well as the proportion of clasts interpreted as Jura and Knockfarril Hill (Section 3.4). The overlying Knockfarril Hill member is exposed to erosion before Jura, allowing descendant clasts to accumulate in the region as the Knockfarril Hill member erodes away.

Figure 4-3 illustrates the proposed lifecycle of clasts in Glen Torridon after eroding from bedrock. Given their frequent appearance near bedrock, angularity and shape reminiscent of cracked bedding layers, Type 1, Type 2 and Type 8 clasts are suspected to be the most freshly loosened clasts. Type 1 clasts form from multiple thin bedding layers sloughing off in unison, while Type 2 clasts are the result of a single thick bedding layer detaching into multiple blocks (e.g. Fig. 4-2a). Attempts to drill into the Jura member at the Aberlady drill site resulted in the uplift of a bedding layer which had a similar morphology as many of the Type 1 clasts observed in this study (Fig. 4-2c, 4-2d). Type 8 clasts appear to be formed predominately by fracturing in the Knockfarril Hill member.

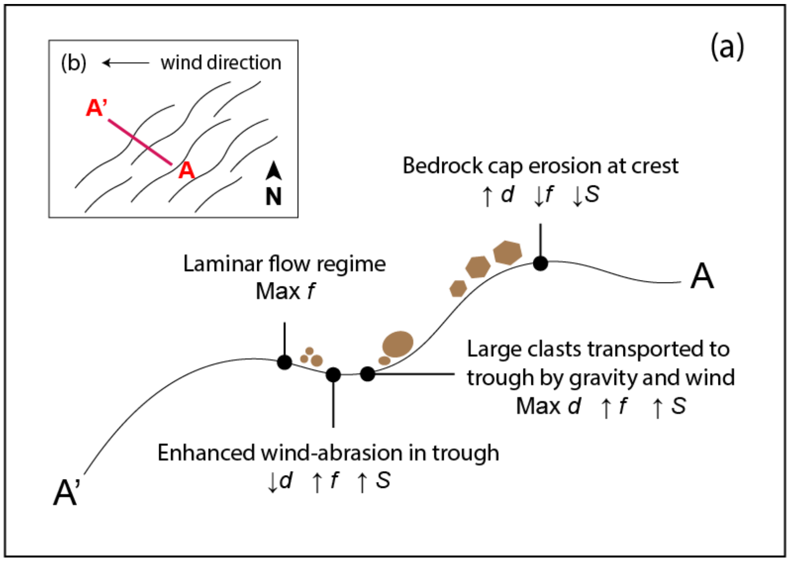

Figure 4-4: (a) Change in clast size and morphology along PBR profile. (b) Representation of Glen Torridon PBR orientation. Present-day wind direction is E-W (Baker et. al., this issue).

Following detachment, clasts are fully exposed to wind abrasion. Type 1 clasts appear to weather into Type 6 clasts, which have similarly high aspect ratios and low solidity values. Type 2 and Type 8 clasts appear to evolve into Type 7 and Type 3 clasts, developing facets and other signs of aeolian wear. These four clast varieties have similar shape characteristics. Type 7 clasts are large and rounded, perhaps in the early stages of facet development. Several Type 3 clasts are observed to have four faces, at least one of which has evolved into a facet – which is consistent with an origin from the rectilinear Type 2 clasts.

While bedrock fragmentation and aeolian abrasion accounts for the vast majority of clasts in Glen Torridon, rounded to well-rounded clasts (i.e. most Type 4 and 5 clasts) are not as easily explained by this process. Aeolian abrasion is only known to round granule-sized clasts over long transport distances (Greeley et al., 2006). It is possible that Type 4 and 5 clasts were transported across the length of Glen Torridon to achieve their degree of rounding, but fluvial transport is the most frequently cited cause for rounded clasts. Though composition indicates the majority of clasts are locally sourced, flooding events or stream channels within the Glen Torridon region could have contributed to clast rounding. A flooding scenario is particularly appealing, since floods could have also deposited the sand required for ventifact formation.

4.4 Relationship to PBRs

The exposed bedrock that is eroding to form the periodic bedrock ridges throughout Glen Torridon is a potential source of new clasts. Trends in shape along the PBR slopes discussed in Section 3.3 suggest clasts are being loosened at the crest by wind and transported downslope, becoming rounder, smoother and more equant. Larger clasts have a tendency to form where Knockfarril Hill member capping units are present. Type 2 and 7 distributions indicate these clasts accumulate along the PBR flanks and develop aeolian features as they migrate away from the crest. Upon reaching the trough, enhanced wind-abrasion erases polish and rounds clasts.

5 Conclusion

Clast morphology and surface features enabled sorting of clasts within Glen Torridon into eight characteristic types. Clast types represent distinct stages along the erosional continuum, displaying signs of increasing aeoliean wear and potentially long-distance transport. The reflection of high *Mg* and high *K* signatures typical of Jura and Knockfarril Hill members, respectively, in clasts sampled throughout Glen Torridon indicate that the clasts are formed in the region. Taking the results of clast morphology, spatial distribution and geochemistry data together, we propose that clasts within Glen Torridon are the result of in-situ bedrock degradation facilitated by aeolian abrasion. Enhanced and directional winds in the troughs and on the slopes of PBRs serve to drive clast smoothing, rounding and mass loss over long timescales.

Future studies may incorporate clast morphology and distribution analysis to determine clast erosion rates, which may help constrain paleowind speeds and directions. Results of such studies may be used to further our understanding of the formation and modification of the periodic bedrock ridges characteristic of the Glen Torridon region.

Acknowledgements

This effort was carried out in part at the Jet Propulsion Laboratory, California Institute of Technology, and at the home institutions of the named co-authors under a contract with the National Aeronautics and Space Administration. The authors would like to acknowledge the scientists and engineers of the MSL Curiosity and HiRISE missions for acquiring and providing the data used in this study. The authors would like to thank and acknowledge the reviewers of this manuscript. Special thanks to Ray Arvidson and Rob Sullivan for their review and revision of this article. Data referenced in this article is available through the NASA Planetary Data System (Edgett, 2013; Malin, 2013; Wiens, 2013).

Bibliography

Anderson, R. (2010). Geologic mapping and characterization of Gale Crater and implications for its potential as a Mars Science Laboratory landing site. *The Mars Journal*, *5*. https://doi.org/10.1555/mars.2010.0004

Atkins, C. B. (2003). *Characteristics of Striae and Clast shape in glacial and non-glacial environments*. Victoria University of Wellington. Retrieved from http://researcharchive.vuw.ac.nz/handle/10063/868

Atkins, C. B. (2004). *Photographic atlas of striae in glacial and non-glacial environments* (Antarctic Data Series Report No. 28). New Zealand: Victoria University of Wellington. Retrieved from http://www.victoria.ac.nz/antarctic/pdf/ADS28.pdf

Baker, M., Lewis, K. W., Bridges, N., Newman, C., Van Beek, J., & Lapotre, M. (2017). AEOLIAN TRANSPORT OF COARSE SEDIMENT IN THE MODERN MARTIAN ENVIRONMENT. Presented at the Dust in the Atmosphere of Mars.

Baker et. al., this issue

Bell III, J. F., Godber, A., Rice, M. S., Fraeman, A., Ehlmann, B. L., Goetz, W., et al. (2013). *INITIAL MULTISPECTRAL IMAGING RESULTS FROM THE MARS SCIENCE LABORATORY MASTCAM INVESTIGATION AT THE GALE CRATER FIELD SITE*. Lunar Planet. Sci. XLIV, 1417 (abstract).

Benn, D., & Evans, D. J. (2014). *Glaciers and glaciation*. Routledge.

Bibring, J.-P., Langevin, Y., Mustard, J. F., Poulet, F., Arvidson, R., Gendrin, A., et al. (2006). Global Mineralogical and Aqueous Mars History Derived from OMEGA/Mars Express Data. *Science*, *312*(5772). https://doi.org/10.1126/science.1122659

Bloom, A. L. (1978). *Geomorphology: A Systematic Analysis of Late Cenozoic Landforms*. Prentice-Hall. Retrieved from https://books.google.com/books?id=IgG1AAAAIAAJ

Boulton, G. (1978). Boulder shapes and grain-size distributions of debris as indicators of transport paths through a glacier and till genesis. *Sedimentology*, *25*(6), 773–799.

Bourke, M., Nicoli, J., Viles, H., & Holmlund, J. (2007). THE PERSISTENCE OF FLUVIAL FEATURES ON CLASTS: RESULTS OF WIND TUNNEL ABRASION EXPERIMENTS. Presented at the LPSC XXXVIII.

Bourke, Mary, & Viles, H. A. (2007). *A Photographic Atlas of Rock Breakdown Features in Geomorphic Environments*.

Bridges, N. T., Greeley, R., Haldemann, A. F. C., Herkenhoff, K. E., Kraft, M., Parker, T. J., & Ward, A. W. (1999). Ventifacts at the Pathfinder landing site. *Journal of Geophysical Research: Planets*, *104*(E4), 8595–8615. https://doi.org/10.1029/98JE02550

Bridges, N. T., Calef, F. J., Hallet, B., Herkenhoff, K. E., Lanza, N. L., Mouélic, S. L., et al. (2014). The rock abrasion record at gale crater: Mars science laboratory results from Bradbury landing to Rocknest. *Journal of Geophysical Research: Planets*, *119*(6), 1374–1389. https://doi.org/10.1002/2013JE004579

Bristow, T. F., Rampe, E. B., Grotzinger, J. P., Fox, V. K., Bennett, K. A., Yen, A. S., et al. (2019). *CLAY MINERALS OF GLEN TORRIDON, MOUNT SHARP, GALE CRATER, MARS*. LPSC IX. 2089 (abstract).

Cailleux, A. (1947). L'indice d'emoussé des grains de sable et grés. *Rev. Geomorphol.*, *Dyn 3*, 78–87.

Cooke, R. U., Warren, A., & Goudie, A. S. (1993). *Desert Geomorphology*. CRC Press. Retrieved from https://books.google.com/books?id=WOcUNbRUGtwC

Cousin, A., Desjardins, M., Dehouck, E., Forni, O., David, G., Berger, G., et al. (2021). *K-Rich Rubbly Bedrock at Glen Torridon, Gale Crater, Mars: Investigating the Possible Presence of Illite*. Lunar Planet. Sci. LII, 2548 (abstract).

Dehouck, E., Cousin, A., Mangold, N., Frydenvang, J., Lasue, J., Meslin, P.-Y., et al. (2019). Geochemistry of the clay-bearing sedimentary rocks of Glen Torridon, Gale crater, Mars. *EPSC*, *13*(979–1).

Deit, L. L., Hauber, E., Fueten, F., Pondrelli, M., Rossi, A. P., & Jaumann, R. (2013). Sequence of infilling events in Gale Crater, Mars: Results from morphology, stratigraphy, and mineralogy. *Journal of Geophysical Research: Planets*, *118*(12). https://doi.org/10.1002/2012JE004322

Durand, M., & Bourquin, S. (2013). Criteria for the identification of ventifacts in the geological record: A review and new insights. *Comptes Rendus Geoscience*, *345*(3). https://doi.org/10.1016/j.crte.2013.02.004

Edgar, L. A., Fedo, C. M., Gupta, S., Banham, S. G., Fraeman, A. A., Grotzinger, J. P., et al. (2020). A Lacustrine Paleoenvironment Recorded at Vera RubinRidge, Gale Crater: Overview of the Sedimentology and Stratigraphy Observed by the Mars ScienceLaboratory Curiosity Rover. *Journal of Geophysical Research: Planets*, *125*(3). https://doi.org/10.1029/2019JE006307

Edgett, K., MSL Mars Hand Lens Imager Camera EDR V1.0, NASA Planetary Data System, MSL-M-MAHLI-2-EDR-IMG-V1.0, 2013.

Fedo, C., Grotzinger, J., Gupta, S., Stein, N. T., Watkins, J., Banham, S., et al. (2017). *FACIES ANALYSIS AND BASIN ARCHITECTURE OF THE UPPER PART OF THE MURRAY FORMATION, GALE CRATER, MARS*. Lunar Planet. Sci. XLVIII, 1689 (abstract).

Fox, V. K., Bennett, K. A., Bryk, A., Arvidson, R., Bristow, T., Dehouck, E., et al. (2020). *One Year in Glen Torridon: Key Results from the Mars Science Laboratory Curiosity Rover exploration of clay-bearing units*. Lunar Planet. Sci. LI, 2833 (abstract).

Fraeman, A. A., Ehlmann, B. L., Arvidson, R. E., Edwards, C. S., Grotzinger, J. P., Milliken, R. E., et al. (2016). The stratigraphy and evolution of lower Mount Sharp from spectral, morphological, and thermophysical orbital data sets. *Journal of Geophysical Research: Planets*, *121*(9). https://doi.org/10.1002/2016JE005095

Fraeman, A. A., Edgar, L. A., Rampe, E. B., Thompson, L. M., Frydenvang, J., Fedo, C. M., et al. (2020). Evidence for a Diagenetic Origin of Vera Rubin Ridge, Gale Crater, Mars: Summary and Synthesis of *Curiosity* 's Exploration Campaign. *Journal of Geophysical Research: Planets*, *125*(12). https://doi.org/10.1029/2020JE006527

Glass, B. P. (1990). Tektites and microtektites: key facts and inferences. *Tectonophysics*, *171*(1), 393–404. https://doi.org/10.1016/0040-1951(90)90112-L

Golombek, M. P., Grant, J. A., Crumpler, L. S., Greeley, R., Arvidson, R. E., Bell, J. F., et al. (2006). Erosion rates at the Mars Exploration Rover landing sites and long-term climate change on Mars. *Journal of Geophysical Research E: Planets*, *111*(12). https://doi.org/10.1029/2006JE002754

Greeley, R. (1984). Abrasion by aeolian particles : Earth and Mars, iv, 50 p. :

Greeley, R., Arvidson, R. E., Elachi, C., Geringer, M. A., Plaut, J. J., Saunders, R. S., et al. (1992). Aeolian features on Venus: Preliminary Magellan results. *Journal of Geophysical Research: Planets*, *97*(E8), 13319–13345. https://doi.org/10.1029/92JE00980

Greeley, R., Kuzmin, R. O., & Haberle, R. M. (2001). Aeolian Processes and their Effects on Understanding the Chronology of Mars. *Space Science Reviews*, *96*(1), 393–404. https://doi.org/10.1023/A:1011917910624

Greeley, R., Arvidson, R. E., Barlett, P. W., Blaney, D., Cabrol, N. A., Christensen, P. R., et al. (2006). Gusev crater: Wind-related features and processes observed by the Mars Exploration Rover Spirit. *Journal of Geophysical Research: Planets*, *111*(E2). https://doi.org/10.1029/2005JE002491

Greeley, Ronald, Bridges, N. T., Kuzmin, R. O., & Laity, J. E. (2002). Terrestrial analogs to wind-related features at the Viking and Pathfinder landing sites on Mars. *Journal of Geophysical Research: Planets*, *107*(E1), 5-1-5–22. https://doi.org/10.1029/2000JE001481

Grotzinger, J. P., Sumner, D. Y., Kah, L. C., Stack, K., Gupta, S., Edgar, L., et al. (2014). *A Habitable Fluvio-Lacustrine Environment at Yellowknife Bay, Gale Crater, Mars*. https://doi.org/10.1126/science.1242777

Grotzinger, J. P., Gupta, S., Malin, M. C., Rubin, D. M., Schieber, J., Siebach, K., et al. (2015). Deposition, exhumation, and paleoclimate of an ancient lake deposit, Gale crater, Mars. *Science*, *350*(6257). https://doi.org/10.1126/science.aac7575

King, L. (1949). Some Remarkable Wind-Faceted Pebbles from near the Mouth of the Umhlangakulu River, Southern Natal, South Africa. *The Journal of Geology*, *57*(4), 413–414. https://doi.org/10.1086/625632

Laity, J. E., & Bridges, N. T. (2009). Ventifacts on Earth and Mars: Analytical, field, and laboratory studies supporting sand abrasion and windward feature development. *Geomorphology*, *105*(3–4). https://doi.org/10.1016/j.geomorph.2008.09.014

Malin, M. C., Ravine, M. A., Caplinger, M. A., Ghaemi, F. T., Schaffner, J. A., Maki, J. N., et al. (2017). The Mars Science Laboratory (MSL) Mast cameras and Descent imager: Investigation and instrument descriptions. *Earth and Space Science*, *4*(8). https://doi.org/10.1002/2016EA000252

Malin, M., MSL Mars Mast Camera EDR V1.0, NASA Planetary Data System, MSL-M-MASTCAM-2-EDR-IMG-V1.0, 2013.

Maurice, S., Wiens, R. C., Saccoccio, M., Barraclough, B., Gasnault, O., Forni, O., et al. (2012). The ChemCam Instrument Suite on the Mars Science Laboratory (MSL) Rover: Science Objectives and Mast Unit Description. *Space Science Reviews*, *170*(1–4). https://doi.org/10.1007/s11214-012-9912-2

McCall, G. J. H. (2001). Tektites in the geological record: showers of glass from the sky. Geological Society of London.

McCauley, J. F., Breed, C. S., El-Baz, F., Whitney, M. I., Grolier, M. J., & Ward, A. W. (1979). Pitted and fluted rocks in the western desert of Egypt: Viking comparisons. *Journal of Geophysical Research: Solid Earth*, *84*(B14), 8222–8232. https://doi.org/10.1029/JB084iB14p08222

Milliken, R. E., Swayze, G. A., Thomson, B. J., Edgett, K. S., Swayze, G., Clark, R. N., et al. (2009). *Clay and sulfate-bearing rocks in a stratigraphic sequence in Gale crater*. Lunar Planet. Sci. XL, 1479 (abstract). Retrieved from https://www.researchgate.net/publication/253083302

Milliken, R. E., Grotzinger, J. P., & Thomson, B. J. (2010). Paleoclimate of Mars as captured by the stratigraphic record in Gale Crater. *Geophysical Research Letters*, *37*(4). https://doi.org/10.1029/2009GL041870

Milliken, R. E., Ewing, R. C., Fischer, W. W., & Hurowitz, J. (2014). Wind-blown sandstones cemented by sulfate and clay minerals in Gale Crater, Mars. *Geophysical Research Letters*, *41*(4). https://doi.org/10.1002/2013GL059097

Minitti, M. E., Malin, M. C., Beek, J. K. V., Caplinger, M., Maki, J. N., Ravine, M., et al. (2019). Distribution of primary and secondary features in the Pahrump Hills outcrop (Gale crater, Mars) as seen in a Mars Descent Imager (MARDI) "sidewalk" mosaic. *Icarus*, *328*. https://doi.org/10.1016/j.icarus.2019.03.005

Newsom, H. E., Mangold, N., Kah, L. C., Williams, J. M., Arvidson, R. E., Stein, N., et al. (2015). Gale crater and impact processes – Curiosity's first 364 Sols on Mars. *Icarus*, *249*, 108–128. https://doi.org/10.1016/j.icarus.2014.10.013

O'connell-Cooper, C. D., Thompson, L. M., Gellert, R., Spray, J. G., Boyd, N. I., Berger, J., et al. (2021). *APXS geochemistry of the fractured Intermediate Unit (fIU)-its relationship to underlying Glen Torridon units and overlying pediment rocks at the Greenheugh unconformity*. Lunar Planet. Sci. LII, 2405 (abstract).

Ollier, C. D. (1965). Dirt cracking - a type of insolation weathering. *Australian Journal of Science*, (27), 236–237.

Olson, E. (2013). Particle Shape Factors and Their Use in Image Analysis – Part 1 : Theory.

Osinski, G. R., & Pierazzo, E. (2012). *Impact Cratering: Processes and Products*. Wiley. Retrieved from https://books.google.com/books?id=PsrtMhr-1gsC

Powers, M. C. (1953). A New Roundness Scale for Sedimentary Particles. *SEPM Journal of Sedimentary Research*, *Vol. 23*. https://doi.org/10.1306/D4269567-2B26-11D7-8648000102C1865D

Riley, N. A. (1941). Projection Sphericity. *SEPM Journal of Sedimentary Research*, *Vol. 11*. https://doi.org/10.1306/D426910C-2B26-11D7-8648000102C1865D

Rivera-Hernández, F., Sumner, D. Y., Mangold, N., Stack, K. M., Forni, O., Newsom, H., et al. (2019). Using ChemCam LIBS data to constrain grain size in rocks on Mars: Proof of concept and application to rocks at Yellowknife Bay and Pahrump Hills, Gale crater. *Icarus*, *321*. https://doi.org/10.1016/j.icarus.2018.10.023

Sautter, V., Fabre, C., Forni, O., Toplis, M. J., Cousin, A., Ollila, A. M., et al. (2014). Igneous mineralogy at Bradbury Rise: The first ChemCam campaign at Gale crater. *Journal of Geophysical Research: Planets*, *119*(1). https://doi.org/10.1002/2013JE004472

Sautter, V., Toplis, M. J., Wiens, R. C., Cousin, A., Fabre, C., Gasnault, O., et al. (2015). In situ evidence for continental crust on early Mars. *Nature Geoscience*, *8*(8). https://doi.org/10.1038/ngeo2474

Sharp, M. (1982). Modification of clasts in lodgement tills by glacial erosion. *Journal of Glaciology*, *28*(100), 475–481.

Spray, J. G., Thompson, L. M., Biren, M. B., & O'Connell-Cooper, C. (2010). The Manicouagan impact structure as a terrestrial analogue site for lunar and martian planetary science. *Planetary and Space Science*, *58*(4), 538–551. https://doi.org/10.1016/j.pss.2009.09.010

Stack, K. M. (n.d.). Orbital and In-Situ Investigation of Periodic Bedrock Ridges in Glen Torridon, Gale Crater, Mars. *Journal of Geophysical Research E: Planets*, (this issue).

Stack, K. M., Grotzinger, J. P., Lamb, M. P., Gupta, S., Rubin, D. M., Kah, L. C., et al. (2019). Evidence for plunging river plume deposits in the Pahrump Hills member of the Murray formation, Gale crater, Mars. *Sedimentology*, *66*(5), 1768–1802. https://doi.org/10.1111/sed.12558

Stack, K. M., Sun, V. Z., Arvidson, R. E., Fedo, C., Day, M., Bennett, K., et al. (2019). *ORIGIN OF LINEAR RIDGES IN THE CLAY-BEARING UNIT OF MOUNT SHARP, GALE CRATER, MARS*. Lunar Planet. Sci. L, 1210 (abstract).

Sullivan, R., & Kok, J. F. (2017). Aeolian saltation on Mars at low wind speeds. *Journal of Geophysical Research: Planets*, *122*(10), 2111–2143. https://doi.org/10.1002/2017JE005275

Sullivan, R., Banfield, D., Bell, J. F. 3rd, Calvin, W., Fike, D., Golombek, M., et al. (2005). Aeolian processes at the Mars Exploration Rover Meridiani Planum landing site. *Nature*, *436*(7047), 58–61. https://doi.org/10.1038/nature03641

Therriault, A. M., Fowler, A. D., & Grieve, R. A. (2002). The Sudbury Igneous Complex: A differentiated impact melt sheet. *Economic Geology*, *97*(7), 1521–1540.

Thomson, B. J., Bridges, N. T., & Greeley, R. (2008). Rock abrasion features in the Columbia Hills, Mars. *Journal of Geophysical Research: Planets*, *113*(E8). https://doi.org/10.1029/2007JE003018

Thomson, B. J., Bridges, N. T., Milliken, R., Baldridge, A., Hook, S. J., Crowley, J. K., et al. (2011). Constraints on the origin and evolution of the layered mound in Gale Crater, Mars using Mars Reconnaissance Orbiter data. *Icarus*, *214*(2). https://doi.org/10.1016/j.icarus.2011.05.002

Wiens, R., MSL ChemCam Laser Induced Breakdown Spectrometer raw data, MSL-M-CHEMCAM-LIBS-2-EDR-V1.0, NASA Planetary Data System, 2013.

Wells, G., & Zimbelman, J. (1997). Extraterrestrial arid surface processes.

Whipple, K. X., & Dunne, T. (1992). The influence of debris-flow rheology on fan morphology, Owens Valley, California. *Geological Society of America Bulletin*, *104*(7). https://doi.org/10.1130/0016-7606(1992)104<0887:TIODFR>2.3.CO;2

Whitney, M. I., & Dietrich, R. V. (1973). Ventifact Sculpture by Windblown Dust. *GSA Bulletin*, *84*(8), 2561–2582. https://doi.org/10.1130/0016-7606(1973)84<2561:VSBWD>2.0.CO;2

Yingst, R. A., Crumpler, L., Farrand, W. H., Li, R., & Souza, P. D. (2010). Constraints on the geologic history of "Home Plate" materials provided by clast morphology and texture. *Journal of Geophysical Research E: Planets*, *115*(12). https://doi.org/10.1029/2010JE003668

Yingst, R. A., Kah, L. C., Palucis, M., Williams, R. M. E., Garvin, J., Bridges, J. C., et al. (2013). Characteristics of pebble- and cobble-sized clasts along the curiosity rover traverse from bradbury landing to rocknest. *Journal of Geophysical Research E: Planets*, *118*(11), 2361–2380. https://doi.org/10.1002/2013JE004435

Yingst, R. A., Cropper, K., Gupta, S., Kah, L. C., Williams, R. M. E., Blank, J., et al. (2016). Characteristics of pebble and cobble-sized clasts along the Curiosity rover traverse from sol 100 to 750: Terrain types, potential sources, and transport mechanisms. *Icarus*, *280*, 72–92. https://doi.org/10.1016/j.icarus.2016.03.001